MATERIALS SCIENCE

Immobilized ^{13}C-labeled polyether chain ends confined to the crystallite surface detected by advanced NMR

Shichen Yuan and Klaus Schmidt-Rohr*

A comprehensive ^{13}C nuclear magnetic resonance (NMR) approach for characterizing the location of chain ends of polyethers and polyesters, at the crystallite surface or in the amorphous layers, is presented. The OH chain ends of polyoxymethylene are labeled with ^{13}COO-acetyl groups and their dynamics probed by ^{13}C NMR with chemical shift anisotropy (CSA) recoupling. At least three-quarters of the chain ends are not mobile dangling cilia but are immobilized, exhibiting a powder pattern characteristic of the crystalline environment and fast CSA dephasing. The location and clustering of the immobilized chain ends are analyzed by spin diffusion. Fast ^{1}H spin diffusion from the amorphous regions shows confinement of chain ends to the crystallite surface, corroborated by fast ^{13}C spin exchange between chain ends. These observations confirm the principle of avoidance of density anomalies, which requires that chains terminate at the crystallite surface to stay out of the crowded interfacial layer.

INTRODUCTION

Chain ends can play an important, if underappreciated, role in the formation and stability of the lamellar semicrystalline morphology of many polymers (*1*). Figure 1 displays four distinct potential distributions of chain ends that have been shown in the literature for five decades but could not be distinguished experimentally except in the special case of polyethylene (PE). While it was speculated early on (*2*) that dangling cilia (see Fig. 1A) of otherwise tightly folded chains give rise to the ~15% mobile amorphous segments almost ubiquitously observed in polymers of high crystallinity, including solution crystals, such structural models often produce crowded interfacial layers with excess density higher than in the crystallites (*1*, *3*, *4*). Such a density anomaly, which arises as chains leave a densely packed crystallite and meander in the disordered interfacial layer, impinging on each other (*1*), is substantially reduced if chains are not only tilted relative to the crystallite surface normal (*1*, *3*, *5*) but also terminate at the crystallite surface so that they avoid entering the crowded interfacial layer (Fig. 1B) (*1*). Chain ends are indeed concentrated at the lamellar surface in monodisperse oligomeric systems, e.g., long-chain *n*-alkanes (*6*) and polyethylene oxide (*7*), after transient noninteger folding has transformed into stable integer folding. A majority of chain ends immobilized at the surface of the crystallites in polydisperse PE have been detected by ^{13}C{^{1}H} and ^{2}H solid-state nuclear magnetic resonance (NMR) (*1*, *8*). Furthermore, with decreased concentration of chain ends due to increased molecular weight, crowding reduction in the interfacial layer requires more pronounced chain tilt relative to the shortest trajectory through the crystallite (*1*, *9*).

Chain ends can reach their thermodynamically favored locations if the chains are sufficiently mobile either during crystallization or in the solid state due to α_C mobility (chain diffusion) (*10*–*12*), which also enables solvent-free PE processing (*13*). In crystal-fixed polymers (*11*), chain ends might be trapped throughout the crystallites. Then, an approximately homogeneous distribution of polymer chain ends throughout the crystalline regions (*14*) should lead to row defects (Fig. 1C) or extensive disorder in the crystallites (Fig. 1D). To date, most studies of the chain-end distribution have focused on PE, an α_C-mobile polymer, and found evidence for the structural features in Fig. 1B (*1*, *6*, *8*). Whether other polymers with different chain mobility (*11*), chain conformation (*1*), interchain interactions (*15*), or crystallization kinetics (*12*, *16*) exhibit different chain-end distributions is not known.

Studies of the spatial distribution of chain ends have been limited (*1*, *8*, *14*, *17*), probably due to the experimental difficulties associated with the low concentration of chain ends. The NMR studies have been based on well-resolved end-group signals (*1*, *14*) or specific block-copolymer synthesis (*8*) particular to PE, which do not generalize to other polymers. Therefore, the development of new approaches to characterize other types of chain ends is desirable. In this study, we analyze chain ends in polyoxymethylene (POM), a relatively hard engineering polymer of high crystallinity that has very slow chain diffusion at 298 K (*18*) and might therefore have a different chain-end distribution than PE. Via acetylation, the "natural" OH chain ends in POM homopolymer can be converted into acetyl groups, which is adopted in industry to prevent thermal degradation of POM (*19*, *20*) and can be generalized to polyesters and other polyethers. Acetyl groups are much less bulky than other chain-end tags such as the (2,2,6,6-tetramethylpiperidin-1-yl)oxyl (TEMPO) group for electron paramagnetic resonance (EPR) studies (*21*) and therefore have no substantial disruptive effect. By acetylation using ^{13}COO-enriched acetic anhydride, the small NMR signal of chain ends can be enhanced 90-fold.

In this work, we demonstrate how the distribution of ^{13}C-labeled acetylated chain ends across the semicrystalline morphology can be studied by a series of state-of-the-art NMR techniques. Contrast in segmental mobility between the nearly rigid crystallites and the mobile amorphous layers is exploited to distinguish chain ends in the crystallites from those in the amorphous regions. The motional narrowing of C-H or H-H wide-line spectra (*22*, *23*) commonly exploited to characterize the motions of CH_2 or CH groups cannot be used here, but for the ^{13}C-enriched esters, the chemical shift anisotropy (CSA) is a good probe of mobility (*24*). Motional narrowing of CSA powder patterns can be detected with isotropic shift resolution in two-dimensional separation of undistorted powder patterns by effortless recoupling (SUPER) (*25*) NMR spectra, while quantification of the mobile chain end fraction is enabled by CSA-dephasing NMR (*26*) after direct polarization (DP). The spectrally resolved immobilized crystalline and mobile amorphous backbone esters in

Department of Chemistry, Brandeis University, Waltham, MA 02453, USA.
*Corresponding author. Email: srohr@brandeis.edu

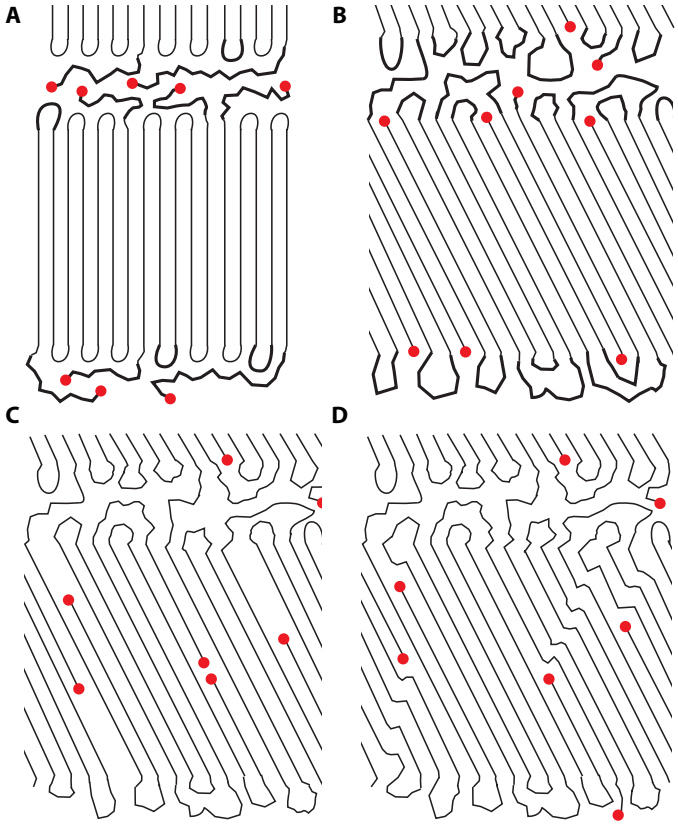

Fig. 1. Schematics of possible locations of chain ends (filled red circles) in the lamellar semicrystalline morphology. Mobile segments (assuming $T >> T_g$) are marked by a greater line thickness. (**A**) Chain ends as dangling cilia. The location of the chain ends in low-density regions deep in the amorphous layers would facilitate their large-amplitude motions. (**B**) Chain ends mostly confined to the crystallite surface, to reduce excess density (*1*) in the folds and loops near the crystalline-amorphous interface. (**C**) Chain ends inside the crystallite generating row vacancy defects. A pair of chain ends is shown in the center of the figure. (**D**) Chain ends inside the crystallite producing kink defects. The crystallite thickness is typically 5 to 30 nm (see also fig. S1).

unlabeled poly(ε-caprolactone) (PCL) are analyzed for reference. Selective detection of end groups with limited mobility is achieved by ^{1}H double-quantum (DQ) filtering (*27*) with ^{13}C detection. The depth of the chain ends from the crystallite surface can be probed by ^{1}H spin diffusion (*28*) after a T_{2H} and chemical shift filter. The clustering of chain ends at the crystallite surface can be detected by centerband-only detection of exchange (CODEX) NMR (*29*) with ^{13}C spin exchange, potentially even in the absence of amorphous-phase mobility. Some properties of the crystallite surface can be probed by analysis of the relative orientation of chain ends concentrated at that surface. The NMR methods demonstrated here can be applied to characterize chain ends in other polyethers and in polyesters originally terminated with OH groups.

RESULTS

Crystallinity and ^{13}COO fraction from quantitative ^{13}C NMR

A quantitative DP ^{13}C NMR spectrum of ^{13}C-Ac$_2$-POM is shown as the top trace in Fig. 2. Quantitative signal intensities were obtained with a recycle delay of 125 s, based on a T_{1C} relaxation time of 20 s

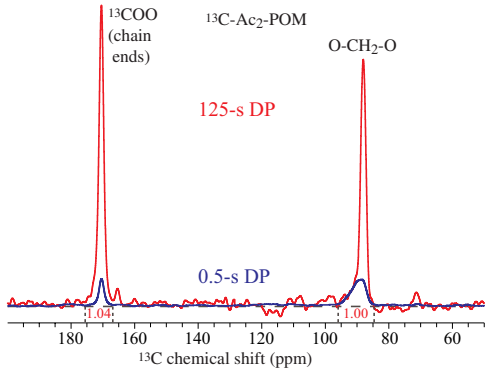

Fig. 2. DP ^{13}C NMR spectra of ^{13}C-Ac$_2$-POM. Top trace (red): Quantitative DP spectrum obtained with a 125-s recycle delay, with an integral ratio of ^{13}COO: O-CH$_2$-O = 1.04:1; note that the chain-end signal is enhanced 90-fold by isotope labeling. Lower trace (blue): Selective DP spectrum of fast-relaxing, mobile O-CH$_2$-O segments obtained with a 0.5-s recycle delay.

in POM (fig. S2) (*30*). The spectrum shows two peaks, one from the ^{13}C-enriched ester groups of the acetyl chain ends, the other due to ^{13}C in natural abundance in the O-CH$_2$-O units of POM. The peak ratio of 1.04:1, combined with the isotopic enrichment factor of 99%/1.1%, yields a concentration of one ^{13}COO end group per 94 O-CH$_2$ units. This corresponds to a number-average molecular weight of M_n = 4.7 kg/mol if ≥90% acetylation of chain ends is assumed. The strong end-group signal in Fig. 2 demonstrates that even with a five times higher molecular weight M_n, the end-group signal strength would be sufficient to be detectable by NMR.

The signal of mobile ^{13}CH$_2$ groups in the amorphous regions of POM can be selected by DP with a short recycle delay, because fast ^{13}C spin-lattice (T_{1C}) relaxation is driven by fluctuating CH dipolar fields with spectral density near the ^{13}C Larmor frequency. The amorphous O-CH$_2$-O signal quantitatively selected using a recycle delay of 0.5 s is shown as the bottom trace in Fig. 2, normalized per scan. The fractional area of the broad O-CH$_2$-O band [between 85 and 95 parts per million (ppm); see fig. S3] corresponds to an amorphicity of 0.3 and thus a crystallinity of 0.7.

Analysis of immobilization of chain ends by CSA recoupling

Solid-state NMR can easily probe the fast, large-amplitude motions that chain ends in dangling cilia (Fig. 1A) would be expected to undergo, in terms of spectral line narrowing. While for CH$_n$ segments motional narrowing of C-H or H-H wide-line spectra (*22*, *23*) can be observed conveniently, for ester groups, the CSA, producing a broad, well-defined powder pattern (*28*, *31*) in the rigid limit, is a particularly good probe of mobility (*24*). A potentially motionally narrowed CSA powder pattern can be obtained for each resolved peak in the magic angle spinning (MAS) ^{13}C NMR spectrum using two-dimensional SUPER (*25*). To demonstrate the rigid-limit ester powder pattern and motional narrowing due to large-amplitude motions, Fig. 3A presents the comparison of patterns extracted from cross-polarization (CP)– and DP-based SUPER spectra of the semicrystalline polyester PCL. The characteristic, broad ester CSA powder pattern at the crystalline resonance (173.6 ppm) of PCL was extracted from a two-dimensional SUPER spectrum (see fig. S4A) after CP from ^{1}H, while the motionally narrowed peak at the amorphous ester resonance (172.8 ppm) was obtained after DP with a short recycle delay. The contrast between the two spectra confirmed that rigid and

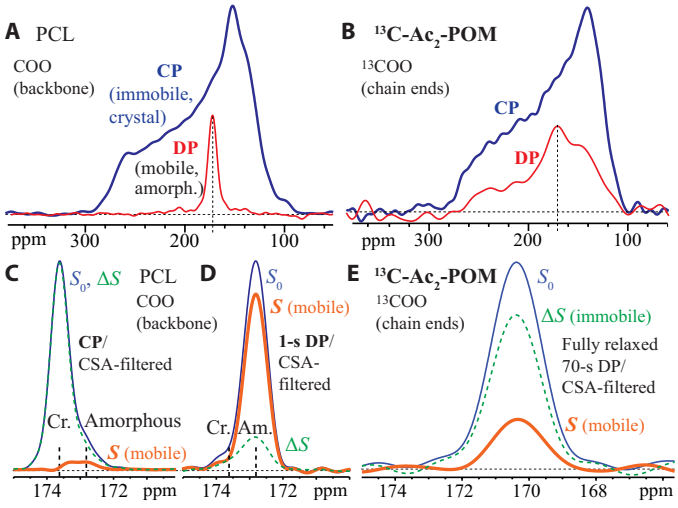

Fig. 3. Immobilized chain ends identified by CSA recoupling. (**A** and **B**) ^{13}C CSA powder spectra of ester groups obtained by SUPER ^{13}C NMR after cross-polarization (CP; top traces, blue, solid-like) and 1-s DP (bottom traces, red). (A) Spectra of the backbone esters in PCL shown for reference, extracted at the crystalline (blue) and amorphous (red) resonance positions. (B) Spectra of the ^{13}COO acetyl chain ends in ^{13}C-Ac$_2$-POM. (**C** to **E**) Separation of ^{13}C NMR signals of immobile and mobile ester groups by a 3 + 2–pulse CSA filter (*26*) with a 32-μs delay between first and second π-pulse. Thick orange line: Spectrum *S* after the CSA filter, from mobile segments with a motionally averaged small CSA. Thin blue line: Full spectrum (S_0) of all esters recorded with CSA dephasing. Dashed green line: Difference $S_0 - S$, mostly of esters with limited mobility. (C) Spectra of crystalline PCL selected by CP. (D) Spectra of mobile, amorphous PCL selected by DP with a 2-s recycle delay. (E) Comprehensive spectra of chain-end ^{13}COO groups in ^{13}C-Ac$_2$-POM with and without CSA filtering, after DP with 70-s recycle delay (fully relaxed).

mobile segments can be separated through CP- and short DP–based experiments, respectively.

Figure 3B displays CSA powder patterns of the rigid and partially mobile chain ends in ^{13}C-Ac$_2$-POM, extracted from CP- and short DP–based SUPER ^{13}C NMR spectra, respectively (see fig. S4B for contour plots of the two-dimensional spectra). The broad, well-defined powder pattern of the chain ends extracted from the CP-based SUPER spectrum spans essentially the same range as the pattern of the PCL crystallites, showing no evidence of fast large-amplitude motions. Even after 0.5-s DP, which selects signals of the most mobile segments as demonstrated for PCL, only a small fraction of end groups produce a narrow peak at the isotropic chemical shift (marked by a dashed vertical line), while most still exhibit residual anisotropic broadening, which excludes fast isotropic motions even for these more mobile POM end groups.

Quantification of the immobilized chain-end fraction is best achieved in terms of relative peak areas in mobility-selective but otherwise quantitative one-dimensional NMR spectra. For CH_n groups in polymers, selective spectra of mobile segments can be obtained by several relaxation-based solid-state NMR techniques, including DP with a short recycle delay as demonstrated above. However, the acetyl chain-end ^{13}COO carbon has weak dipolar couplings to protons, which makes T_{1C} and T_{CH} relaxation of mobile segments less distinctive. On the other hand, the much larger CSA of rigid crystalline COO segments compared to highly mobile esters can be exploited in a CSA filter (*26*), which suppresses the rigid while retaining the mobile COO signals because the apparent transverse relaxation time is inversely proportional to the width of the CSA powder spectrum. While in regular MAS the CSA effect is time-averaged to zero, during a CSA filter, it is recoupled by three rotation-synchronized π-pulses that interfere with its averaging by MAS (*26*).

For reference, Fig. 3 (C and D) demonstrates the effect of a CSA filter with a 32-μs spacing of the first two π-pulses on the COO segments in crystalline (173.6 ppm, polarized by 1.1-ms CP) and amorphous (172.8 ppm, polarized by DP with 1-s recycle delay) components in PCL, respectively. For rigid COO groups detected after CP, complete suppression of signal intensity is observed (CSA-filtered signal *S* in Fig. 3C). Conversely, most magnetization of mobile COOs polarized by 1-s DP passes the 32-μs CSA filter, and ~88% of the amorphous COO peak remains (see Fig. 3D). The observed marked differences between CP- and DP-based spectra confirm that only mobile COO groups can survive the CSA filter.

The same 32-μs CSA filter proven to effectively dephase the rigid ester signal was applied to ^{13}C-Ac$_2$-POM after DP with a 70-s recycle delay, as demonstrated in Fig. 3E. Because T_{1C} of chain-end COO, driven by the fluctuating fields of the nearby rotating acetyl methyl group, is ~7 s, DP with a 70-s recycle delay can comprehensively polarize chain-end COO groups in both crystalline and amorphous regions with negligible bias. Figure 3E shows the COO signal obtained with (S) and without (S_0) 32-μs CSA filtering. The ratio of S/S_0, representing the mobile COO chain-end fraction, is ~25%. This leads to the conclusion that about 75% of the chain ends are immobilized.

Signals of immobilized segments by quasi-static ^{1}H DQ filtering

Selection of signal of chain ends with little mobility, complementary to CSA filtering, can be achieved by ^{1}H quasi-static DQ filtering at 4-kHz MAS. For rigid CH_2 groups, the strong ^{1}H-^{1}H dipolar couplings quickly generate two-spin coherences that can be converted to DQ coherences and selectively back to ^{1}H magnetization, whereas the motionally averaged dipolar couplings of highly mobile segments are too weak to generate such coherences in the given short time. With only 2 × 6 μs of ^{1}H homonuclear dipolar DQ coherence excitation and reconversion, chemical shift evolution and the change in rotor orientation can also be neglected. Through short 0.4-ms CP, the magnetization of the rigid ^{1}H-^{1}H spin pairs is transferred to nearby chain-end COO groups. A more extensive discussion of the pulse sequence can be found in the Supplementary Materials.

Figure 4 (A and B) demonstrates the successful selection of ^{1}H magnetization of immobilized CH_2 groups and suppression of signals of mobile segments in branched PE and in PCL, two semicrystalline polymers with substantial amorphous fractions. The amorphous methylene signals at 31.0 and 64.2 ppm, respectively, detected in the quantitative spectra (top traces) and the 0.4-ms CP spectra (middle traces) are almost completely suppressed by applying the 2 × 6–μs quasi-static DQ filter (bottom traces). These results confirm that the quasi-static DQ filter can select the ^{1}H magnetization of CH_2 groups in a rigid crystalline environment.

The spectrum of ^{13}C-Ac$_2$-POM after 2 × 6–μs quasi-static ^{1}H DQ filtering and CP is shown as the bottom trace (red line) in Fig. 4C. About 41% of the intensity of the broad amorphous O-CH_2-O band is seen to be suppressed [see fig. S3 (C to E) for a deconvolution analysis], which indicates that only a limited fraction of the O-CH_2-O segments in the amorphous layer are highly mobile. The relative

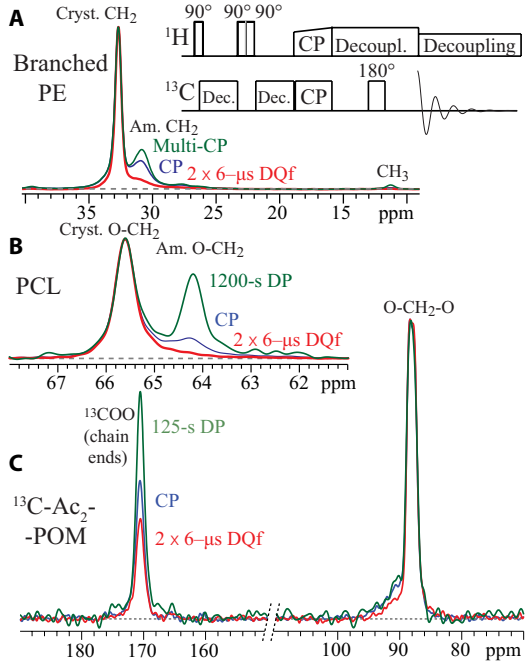

Fig. 4. Selection of signals of immobilized segments by quasi-static ^{1}H DQ filtering for 2 × 6 µs, followed by 0.4-ms CP to ^{13}C. Spinning frequency: 4 kHz. The inset shows the pulse sequence; for details, see the Supplementary Materials. (**A** and **B**) Demonstration of successful suppression of signals of mobile amorphous segments in (A) PE with 2.4 mole percent ethyl branches and (B) PCL (O-CH_2 resonance). In addition to an unselective spectrum with the same CP time (middle, blue trace), a quantitative DP or multi-CP spectrum is also shown (top, green trace in each figure). DQf, DQ filtered. (**C**) Application to ^{13}C-Ac_2-POM.

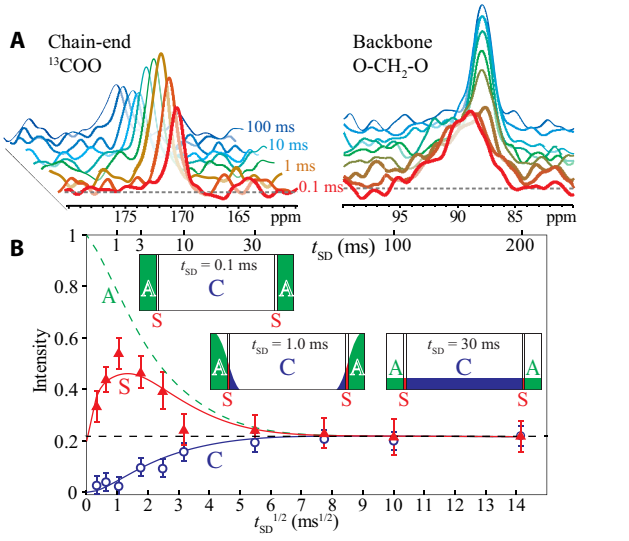

Fig. 5. ^{13}C-detected ^{1}H spin diffusion from the amorphous regions in ^{13}C-Ac_2-POM. (**A**) Series of spectra of the COO and O-CH_2-O signals as a function of spin diffusion time, after 200 µs of T_{2H} filtering that removes the crystalline ^{1}H magnetization and chemical shift filtering that suppresses the CH_3 ^{1}H magnetization, at 10-kHz MAS. (**B**) Time evolution of the chain-end ^{13}COO resonance (filled triangles, top trace) and crystalline O-CH_2-O resonance (open circles, bottom trace) as a function of the square root of the ^{1}H spin diffusion time. The curves show the simulated time dependences of magnetization in the amorphous (dashed), surface (red), and crystalline (blue) regions. The magnetization distribution at three time points is shown schematically in the insets, explaining the maximum of the surface magnetization at t_{SD} = 1 ms.

intensities of the COO signals near 170 ppm show that of all the chain-end esters that are cross-polarizable, ~75% are in a sufficiently immobile environment to pass the quasi-static DQ filter, which is consistent with the immobile fraction of ~75% deduced from CSA dephasing.

Probing the distribution of chain ends across the crystals by ^{1}H spin diffusion

The distribution of chain ends in the crystallites can be probed by ^{1}H spin diffusion (*28*) from the amorphous to the crystalline regions. If the chain ends were uniformly distributed throughout the crystallites, as in Fig. 1 (C and D), then their signal would recover by spin diffusion in parallel with that of the crystalline O-CH_2-O groups. On the other hand, if chain ends are localized at the crystallite surface, as in Fig. 1B, then they are reached earlier by the magnetization transfer from the amorphous regions, and their signals reappear earlier. The magnetization level change at the crystallite surface is particularly distinct from that in the bulk of the crystallite if the amorphous source fraction is <50%, as is the case in POM: Not only does the magnetization at the crystallite surface initially increase quickly, but it later also drops as the magnetization drains into the interior of the crystallite. A resulting maximum (*32*) is characteristic of segments at the crystallite surface.

To start off the spin diffusion experiment with ^{1}H magnetization only in the mobile O-CH_2-O segments, a T_{2H} filter of 200-µs duration (*32*) can be applied on-resonance; it also serves as a chemical shift filter to suppress the magnetization of the acetyl CH_3 groups, which may otherwise be incompletely suppressed because they undergo fast rotational jumps that increase their T_{2H} relaxation time. ^{1}H spin diffusion from the selected amorphous to the rigid components occurs during the spin diffusion time t_{SD} after the T_{2H} filter and before cross polarization to ^{13}C. After the shortest spin diffusion times (t_{SD} < 0.11 ms), only the characteristic broad line shape of the amorphous O-CH_2-O segments near 90 ppm is observed (see Fig. 5A and fig. S3B), which confirms successful selection of magnetization in the noncrystalline regions. Increasing t_{SD} allows for the transfer of ^{1}H magnetization to the crystalline component and a corresponding loss of ^{1}H magnetization in the amorphous component. Consequently, the sharp crystalline O-CH_2-O peak gradually reappears, while the intensity of the broad O-CH_2-O band decreases. Asymptotic values are reached within 50 ms. The spectra at long spin diffusion times of ≥100 ms are identical to the line shape of the unselective CP spectrum, indicating full equilibration of the magnetization by the spin diffusion process. Figure 5B summarizes the time evolution of the intensity of the chain-end ^{13}COO and the deconvolved crystalline O-CH_2-O signals as a function of the square root of the spin diffusion time, because this results in nearly linear initial increases. The vertical scaling in the figure gives the magnetization per ^{1}H spin, with the equilibrium level of 0.22 (the estimated mobile amorphous fraction selected by the T_{2H} filter; see also fig. S6).

The buildup of the chain-end COO signal with t_{SD} is characteristically different from that of the crystalline O-CH_2-O peak. It exhibits a fast increase with t_{SD} in the initial spin diffusion process, reaches a maximum at t_{SD} ~ 1 ms, and then gradually decreases to the equilibrium level at t_{SD} ≥ 10 ms. The initial buildup rate of signal of immobilized chain ends (~0.25 $ms^{-1/2}$) is much larger than that of the crystallite peak (~0.06 $ms^{-1/2}$), which indicates that most

of the immobilized chain ends are spatially close to the amorphous regions, i.e., concentrated at the crystallite surface.

Simulations of the spin diffusion after the T_{2H} filtering can provide more insight into the width of the surface chain-end distribution. Using a spin diffusion model with amorphous, surface, and crystalline layer thicknesses of 1.75, 0.25, and 6.25 nm, respectively (simulation details can be found in the Supplementary Materials), the simulated buildups for surface COO and crystalline O-CH_2-O fit the experimental data. The pronounced maximum in the COO group magnetization can only be reproduced if the immobilized ^{13}COO chain ends are concentrated in a thin layer at the crystallite surface.

Close contacts among chain ends detected by CODEX ^{13}C NMR

Clustering of ^{13}COO chain ends at the crystallite surface can be probed by CODEX ^{13}C NMR with dipolar ^{13}C spin exchange (*29*). CODEX can detect magnetization transfer between ^{13}C spins in differently oriented, magnetically inequivalent COO segments. Dipolar-driven spin exchange occurs faster the closer the ^{13}COO groups, due to the strong distance dependence of the ^{13}C-^{13}C dipolar couplings (*33*). Chain ends that concentrate at the crystallite surface introduce closer contacts among ^{13}COO groups than if the ^{13}COO groups were uniformly distributed in the bulk, thereby resulting in relatively fast ^{13}C-^{13}C spin exchange. Such spin exchange can be detected in CODEX experiments (*29*), where ^{13}C magnetization dephased by CSA recoupling will not refocus into a stimulated echo after the mixing time if spin exchange to a ^{13}C site with a different segmental orientation has occurred.

For ^{13}C-Ac_2-POM, the normalized CODEX signal S/S_0 of chain-end ^{13}COO groups as a function of the mixing time t_m is shown in Fig. 6A. This represents the fraction of chain-end ^{13}C magnetization retaining the same orientation-dependent chemical shift after spin exchange for a time t_m. Spin exchange between magnetically inequivalent ^{13}COO groups driven by dipolar couplings leads to a pronounced decay of S/S_0 as a function of t_m, if the CSA dephasing and refocusing time Nt_r is sufficiently long. The S/S_0 values with Nt_r = 1.2 and 2.4 ms were similar, indicating that the asymptotic limit (*29*) has been reached within the 1.2 ms of CSA recoupling used in the experiments. The S/S_0 ratio decays very fast initially as a function of t_m, with a rate of ca. 0.7 s^{-1}, which indicates close contact among magnetically inequivalent ^{13}COO end groups. In addition, S/S_0 decays to as low as 0.3 within a mixing time of 5 s, which indicates that more than two other magnetically inequivalent sites are nearby (*29*).

To confirm that the decay is caused by spin exchange instead of molecular motion, we performed two additional series of CODEX experiments at higher MAS frequencies of 12.5 and 20 kHz. While the CODEX decay would stay unchanged if the exchange was due to motions, dipolar exchange is slowed down by faster MAS (*34*). Figure S7 shows the experimental decays at 5-, 12.5-, and 20-kHz MAS. With increasing MAS frequency and constant Nt_r = 0.8 ms, the S/S_0 decay was considerably slowed down, proving that the exchange process at 5-kHz MAS is dominated by dipolar spin exchange. It can therefore be analyzed using spin-exchange theory as discussed below.

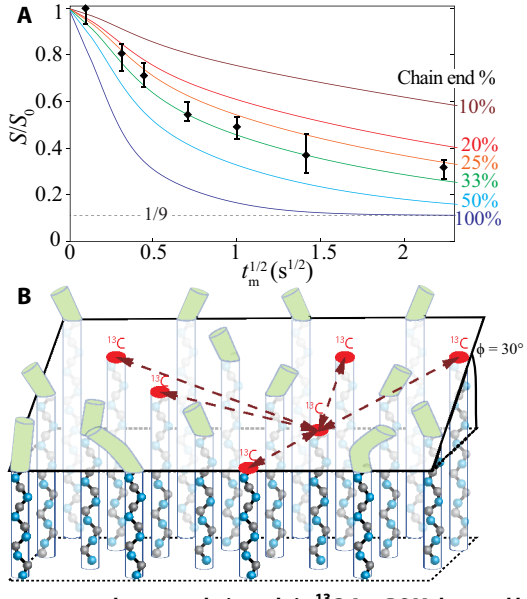

Fig. 6. Close contacts between chain ends in ^{13}C-Ac_2-POM detected by CODEX ^{13}C NMR with dipolar spin exchange. (**A**) Normalized CODEX ^{13}C NMR signal (S/S_0) as a function of the square root of the ^{13}C spin-exchange mixing time ($t_m^{1/2}$), up to t_m = 5 s. A good fit of the CODEX decay is achieved with ~30% of the chains on the crystallite surface terminated by ^{13}C-Ac groups when the surface is a (2 $\bar{1}$ 14) face of the POM crystal (see the Supplementary Materials for simulation details). Because there are nine distinct orientations of segments on the 9_5 helix of POM, the intensity at long t_m approaches 1/9. (**B**) Schematic illustration of the distribution of chain ends (red) on a crystallite surface that is a (2 $\bar{1}$ 14) plane in the crystal structure of POM. The chains in the crystallite are tilted relative to the normal of the crystallite surface (black outlined quadrangle). The chains continuing from the crystallite into the interfacial layer are indicated by green column segments close to the crystallite surface.

DISCUSSION

Immobilized chain ends at the crystallite surface

Cartoons like those in Fig. 1 have been shown in the literature for over 50 years, but experimental data confirming them or ruling them out have been scarce. The current study has shown various lines of evidence that ~75% of chain ends in POM are essentially immobilized at the crystallite surface. Because T_g of POM is ~70 K below room temperature, chain ends terminating in flexible cilia in the amorphous region as depicted in Fig. 1A should be highly mobile. They should then give rise to a narrow peak like the CSA line shape extracted from short DP–based SUPER experiments (see Fig. 3A), would not be expected to produce signal after a short DQ filter, and during spin diffusion out of the mobile regions, their signal should consistently decrease. However, the data from the mobility filtering experiments show none of these behaviors, revealing that most chain ends are not mobile. While the ^{13}C-Ac_2-POM for which the new approach was demonstrated here has only a rather small and inconspicuous mobile amorphous layer, the incorporation of the ester groups into an immobilized solid-like environment observed here does show that the end group is not forced into the most mobile amorphous layer. Both ^{1}H and ^{13}C spin diffusion experiments show strong evidence of immobilized chain ends concentrated at the surface of the crystalline regions, which agrees with the schematic presented in Fig. 1B.

Probing the spatial distribution of chain ends by ^{1}H and ^{13}C spin diffusion

Simulations of ^{1}H spin diffusion in Fig. 5B show that the observed chain-end buildup behavior can only be matched if immobilized chain ends are concentrated in a thin layer at the crystallite surface.

The simulations shown in Fig. 5B indicate amorphous, surface, and crystalline layer thicknesses of 1.75, 0.25, and 6.25 nm, respectively. With a long period of ~8.5 nm from small-angle x-ray scattering (SAXS; fig. S1) and a chain contour length of ~30 nm based on the chain-end concentration, a typical chain traverses a crystallite approximately three times. It therefore crosses the interface six times, out of which two can correspond to ^{13}COO chain ends (*1*). The resulting chain-end concentration at the crystallite surface would be up to about 2/6 = 33%.

According to the crystal structure of POM, in the absence of chain tilt, all segments at the crystallite surface have the same orientation and therefore the same NMR frequency (see fig. S9A). Because CODEX reflects frequency change due to spin exchange, without chain tilt, no major CODEX decay would be observed for chain ends at the crystallite surface, in notable contrast with the experimental results. Otherwise put, the CODEX data indicate chain tilt relative to the local lamellar normal (see fig. S9B), which is in agreement with a ~30° tilt angle of POM chains observed after roll-milling (*35*). Note that the anisotropic chemical shift in the CODEX experiment does not specifically probe the chain-axis direction but would change if the POM helix was rotated around its axis (*18*). Thus, the different chain ends in Fig. 1B would mostly have different frequencies.

The observed initial CODEX dephasing in Fig. 6A is unexpectedly fast, indicating many close approaches among ^{13}COO end groups. A detailed inspection of the POM unit cell shows that the closest inter-stem ^{13}C-^{13}C contact is ~3.7 Å for two adjacent stems on the (1 0 0) face [the crystal growth front (*36*)]. A crystallite surface cleaved along a (2 $\bar{1}$ 14) plane contains the closest inter-stem ^{13}C-^{13}C pair and matches the chain tilt and crystal growth face conditions. For ^{13}COO chain ends in such a (2 $\bar{1}$ 14) plane, simulations of ^{13}C-^{13}C spin exchange were performed with various ^{13}COO chain-end fractions ranging from 100% (all segments at the crystallite surface are chain ends) to 10%; details on the CODEX simulations can be found in the Supplementary Materials. The resulting decay curves are presented in Fig. 6A. The best agreement is obtained for 25 to 33% ^{13}COO chain ends randomly distributed in the plane (see Fig. 6B). This is consistent with the value of 2/6 = 33% chain ends at the crystallite surface obtained for a typical POM chain passing through the crystallite three times, if one takes into account the ~25% chain ends in the amorphous layer, which correspondingly reduces the chain-end fraction at the crystallite surface.

The model in Fig. 6B may seem to lack the roughness of crystallite surfaces observed experimentally (*37*). We propose that chain ends are only moderately disordered because we attribute the roughness mostly to the complex connectivity of chains across the crystalline-noncrystalline interface, resulting in tight folds for adjacent reentry, loops for nonadjacent reentry, entangled loops, tie molecules, crowding problems (*1*), etc. Chain ends at the crystallite surface are not subject to any of these disorder-inducing connectivity effects. We expect neighboring chain ends, which are probed by the CODEX NMR experiment, to be all found near the local crystallite surface because this avoids the formation of vacancies. The close approaches between chain ends and their sharp depth profile observed here are inconsistent with substantial random chain-end displacements into and out of the crystallite that would be associated with surface roughness involving chain ends. The data also clearly exclude dispersal of a substantial fraction (>10%) of chain ends throughout the crystal as in Fig. 1 (C and D).

The chain-end ^{13}C-acetylation approach

The functionalization of polymer chain ends with strong-signal tags presented here overcomes the low signal-to-noise ratio that has been the main hurdle to the characterization of these low-concentration species. The approach is simpler than previous chain-end chemical modifications, some of which required demanding chemical reactions [e.g., anionic polymerization of isotopically labeled monomers (*8*, *38*)]. Other end groups giving strong signals, such as stable-radical (TEMPO) end caps, are too bulky to fit into the crystalline lattice (*21*). The acetyl end group used here, first introduced as a chain-end stabilizer for POM (*19*), not only is small enough to be considered as a regular chain end but also is chemically convenient to produce. It has long been used in industrial polymers without substantial detrimental effects on physical properties. Our data indicate that chain-end ^{13}COO labeling enables the characterization of properties of chain ends by a series of solid-state NMR techniques with adequate signal-to-noise ratio for number-average molecular weights exceeding 30 kg/mol. The approach can be applied to other polyethers and to polyesters.

CONCLUSIONS

An approach combining ^{13}C-labeling of chain ends and a variety of modern NMR experiments for probing the distribution of the chain ends in the semicrystalline morphology has been demonstrated in POM. The convenient ^{13}C-labeling scheme via acetylation is also applicable, with minor variations, to other OH-terminated polymers, which include not only other polyethers but also polyesters. The hypothesis of dangling chain ends or cilia of otherwise tightly folded chains giving rise to the ~15% mobile segments in highly crystalline homopolymers, previously falsified for high-density PE, has been disproved here again, in a different polymer. The CSA powder patterns and dephasing data demonstrate the spectral characteristics of nearly immobilized chain ends, which provide a useful reference for other polymers with highly mobile acetyl chain ends, as observed in ongoing studies in our laboratory. The location of the chain ends at the crystallite surface was documented by an unusual maximum in the chain-end magnetization as a function of ^{1}H spin diffusion time. The clustering of the ^{13}C-labeled chain ends resulting from their confinement to thin layers at the crystallite surfaces was confirmed by fast and extensive ^{13}C-^{13}C spin exchange detected by CODEX NMR. The present study demonstrates that even when crystalline and noncrystalline acetyl chain ends do not exhibit a detectable chemical shift difference, modern mobility– and spin diffusion–based NMR can identify and quantify crystal-immobilized chain ends. A better understanding of the distribution of chain ends promises to shed more light on the crystallization process of semicrystalline polymers.

MATERIALS AND METHODS

Materials

1,3,5-Trioxane (99%), *n*-hexane, *N*,*N*-dimethylcyclohexylamine, and PCL (M_n = 10 kg/mol) were purchased from Sigma-Aldrich; methanol, acetone, and unlabeled palmitic acid from Thermo Fisher Scientific; and acetic anhydride (1,1′-^{13}C, 99%) and 1-^{13}C-palmitic acid from Cambridge Isotope Laboratories. Calcium hydride (93%) was purchased from Acros Organics and boron trifluoride diethyl ether (98+%) from Alfa Aesar. The branched PE (hydrogenated polybutadiene) with M_n = 15 kg/mol has been described in (*39*).

Synthesis of POM

1,3,5-Trioxane was purified by sublimation under atmospheric pressure at 50°C. The resulting needle crystallites (0.5 g) were transferred into a 50-ml oven-dried flask containing 25 ml of *n*-hexane dried over CaH_2 reflux, which was sealed using a rubber septum. Trioxane crystallites were fully dissolved by heating the solution to 50°C under atmospheric pressure (using a dry-air balloon), which was followed by injecting 0.1 ml of BF_3-etherate *n*-hexane solution (0.1 M) through septa while shaking. After a short period of time, the atmosphere above the solution became cloudy. The solution was then kept at 45°C for 12 hours, allowing the polymerization to complete. The residual cations in the POM samples were quenched by boiling with and precipitation from acetone twice (each time for 20 min). The final product was filtered and dried in a fume hood overnight at room temperature (*20*).

Chain-end acetylation

POM powder (0.1 g), together with 0.2 ml of 1-^{13}C-(acetic anhydride), and 60 μl of *N*,*N*-dimethylcyclohexylamine were frozen, then flame sealed under vacuum in a glass ampoule, heated to 200°C to form a melt, and kept at 180°C for the acetylation reaction to occur for 30 min. The melt was gradually brought to room temperature. The solidified product in the ampoule was dissolved in methanol to react with an excess amount of the ^{13}COO-labeled acetic anhydride. The precipitated powder was filtered out and washed twice with methanol. The remaining white powder was then boiled with acetone for 1 hour while stirring and filtered off under suction until the polymer was odorless (*19*). The white powder product was dried overnight in a fume hood and kept in a desiccator with K_2CO_3 for 1 day before being packed into a Kel-F insert of a 4-mm–outer diameter MAS rotor. This material is termed ^{13}C-Ac_2-POM in this paper. For CODEX NMR at several different spinning frequencies, the ^{13}C-Ac_2-POM sample was transferred to a 2.5-mm rotor. The same acetylation procedure was repeated with regular (unlabeled) acetic anhydride to give the Ac_2-POM sample used in SAXS measurements.

Small-angle x-ray scattering

A transmission SAXS measurement on Ac_2-POM was conducted using the Pilatus3 R 300K detector on the SAXSLAB instrument at the Massachusetts Institute of Technology. The x-ray wavelength was $\lambda(CuK_{\alpha 1}) = 1.54$ Å, generated with full power of 45 kV and 0.66 mA. The sample-to-detector distance was 459.1 mm. The sample was sealed in a quartz capillary, and the measurement was taken at room temperature for 5 min.

Nuclear magnetic resonance

Experiments were performed using a Bruker Avance Neo 400WB NMR spectrometer at a ^{13}C resonance frequency of 100 MHz. Most of the measurements were conducted using a Bruker double-resonance MAS probe with 4-mm zirconia rotors. The ^{13}C-Ac_2-POM sample was loaded in a Kel-F insert. The typical B_1 field strength used in CP was 58 kHz, and the radio frequency (rf) field strengths were 69 and 63 kHz for ^{1}H and ^{13}C pulses, respectively. Pulsed ^{1}H decoupling was applied during the echo and acquisition periods with field strengths of $\gamma B_1/2\pi = 95$ and 85 kHz, respectively. The typical recycle delays for CP-based experiments were 6, 6, 2, and 20 s for ^{13}C-Ac_2-POM, PCL, PE (branched), and 1-^{13}C-palmitic acid samples, respectively. ^{13}C chemical shifts were referenced to the α-1-^{13}C-glycine COO resonance at 176.46 ppm. All NMR data were acquired at approximately 300 K. The MAS frequency for ^{13}C-Ac_2-POM was 10 kHz unless otherwise noted.

For ^{13}C DP NMR experiments, recycle delays were set to 125 s with 512 scans, and 0.5 s with 16,384 scans, for the quantitative spectrum and the spectrum of mobile CH_2 groups, respectively, of ^{13}C-Ac_2-POM. The Kel-F insert signal near 110 ppm was removed by subtracting the spectrum of an empty insert with the same number of scans.

The SUPER (*25*) experiments were conducted at a MAS frequency of 5 kHz, after 0.4-ms CP or DP with a 1-s recycle delay, which selects rigid or mobile segments, respectively.

For CSA filtering with 3 + 2 pulses (*26*) at 10-kHz MAS, DP with a 70-s recycle delay was adopted to comprehensively excite the ^{13}C magnetization of ^{13}C-Ac_2-POM. For selecting rigid or mobile segments of PCL, 1.1-ms CP or DP with a 1-s recycle delay, respectively, was used before the CSA filter. For quasi-static ^{1}H DQ filtering with ^{13}C detection, slow spinning at a MAS frequency of 4 kHz was used to ensure that the 2 × 6–μs DQ generation and reconversion were applied to a barely rotated sample. The detailed phase cycling in the pulse sequence (Fig. 4, inset) is listed in table S1. Deconvolution of O-CH_2-O peaks was performed using the MultiPeakFit package in Igor Pro 5.0.3 assuming Gaussian peak shapes. The amorphous and crystalline peaks were determined from selective spectra and the CP spectrum, respectively, and the resulting peak positions and widths were held fixed when deconvolving other spectra.

Experiments with ^{1}H spin diffusion after T_{2H} filtering [Goldman-Shen experiment (*40*, *41*)] and CP to ^{13}C were used to detect the location of the immobilized chain ends relative to the crystallite surface. During the T_{2H} filter of 200-μs duration, the C-H dipolar interaction was decoupled by irradiation at the ^{13}C frequency with a field strength of 43 kHz. The 200-μs evolution was also used as a chemical shift filter to suppress the ^{1}H magnetization of the methyl groups in the acetyl chain ends, with the ^{1}H on-resonance frequency set to 4 ppm. The mixing time for ^{1}H spin diffusion after the T_{2H} filter and before CP ranged from 10 μs to 300 ms.

The CODEX (*29*) experiment was performed at a 5-kHz MAS frequency. Mixing times between 10 ms and 5 s were used. The large CSA of chain-end COO and palmitic acid COOH groups enabled fast dephasing of magnetization in the evolution period. It was confirmed experimentally that $Nt_r = 1.2$ ms (with 2 × 5 π-pulses) and $Nt_r = 2.4$ ms (with 2 × 11 π-pulses) produced almost the same dephasing (long-time limit).

To confirm that the origin of the fast CODEX dephasing in ^{13}C-Ac_2-POM was dipolar-driven spin exchange rather than molecular motion (*34*), CODEX experiments were also performed in a double-resonance probe with a 2.5-mm zirconia rotor at MAS frequencies of 5, 12.5, and 20 kHz, with fixed $Nt_r = 0.8$ ms. The ^{13}C 180° pulse length was as short as possible, 5 μs, at MAS frequencies of 12.5 and 20 kHz and correspondingly somewhat longer, 8 μs, at 5-kHz MAS. The rf field strength for ^{1}H decoupling was 69 kHz.

SUPPLEMENTARY MATERIALS

Supplementary material for this article is available at http://advances.sciencemag.org/cgi/content/full/6/37/eabc0059/DC1

REFERENCES AND NOTES

1. K. J. Fritzsching, K. Mao, K. Schmidt-Rohr, Avoidance of density anomalies as a structural principle for semicrystalline polymers: The importance of chain ends and chain tilt. *Macromolecules* **50**, 1521–1540 (2017).
2. A. Keller, Polymer crystals. *Rep. Prog. Phys.* **31**, 623–704 (1968).

3. M. Hütter, P. J. In 't Veld, G. C. Rutledge, Polyethylene {201} crystal surface: Interface stresses and thermodynamics. *Polymer* **47**, 5494–5504 (2006).
4. C. M. Guttman, J. D. Hoffman, E. A. DiMarzio, Monte Carlo calculation of SANS for various models of semicrystalline polyethylene. *Faraday Discuss. Chem. Soc.* **68**, 297–309 (1979).
5. F. C. Frank, General introduction. *Faraday Discuss. Chem. Soc.* **68**, 7–13 (1979).
6. G. Ungar, X.-b. Zeng, Learning polymer crystallization with the aid of linear, branched and cyclic model compounds. *Chem. Rev.* **101**, 4157–4188 (2001).
7. S. Z. D. Cheng, J. Chen, A. Zhang, D. P. Heberer, Nonintegral and integral folding crystal growth in low-molecular mass poly(ethylene oxide) fractions. II. End-group effect: α,ω-Methoxy-poly(ethylene oxide). *J. Polym. Sci. B* **29**, 299–310 (1991).
8. C. Wutz, M. J. Tanner, M. Brookhart, E. T. Samulski, Where are the chain ends in semicrystalline polyethylene? *Macromolecules* **50**, 9066–9070 (2017).
9. R. G. Alamo, E. K. M. Chan, L. Mandelkern, I. G. Voigt-Martin, Influence of molecular weight on the melting and phase structure of random copolymers of ethylene. *Macromolecules* **25**, 6381–6394 (1992).
10. K. Schmidt-Rohr, H. W. Spiess, Chain diffusion between crystalline and amorphous regions in polyethylene detected by 2D exchange ^{13}C NMR. *Macromolecules* **24**, 5288–5293 (1991).
11. W.-G. Hu, K. Schmidt-Rohr, Polymer ultradrawability: The crucial role of α-relaxation chain mobility in the crystallites. *Acta Polym.* **50**, 271–285 (1999).
12. K. Schäler, A. Achilles, R. Bärenwald, C. Hackel, K. Saalwächter, Dynamics in crystallites of poly(ε-caprolactone) as investigated by solid-state NMR. *Macromolecules* **46**, 7818–7825 (2013).
13. S. Rastogi, Y. Yao, S. Ronca, J. Bos, J. van der Eem, Unprecedented high-modulus high-strength tapes and films of ultrahigh molecular weight polyethylene via solvent-free route. *Macromolecules* **44**, 5558–5568 (2011).
14. E. Pérez, D. L. Vanderhart, Morphological partitioning of chain ends and methyl branches in melt-crystallized polyethylene by ^{13}C-NMR. *J. Polym. Sci. B* **25**, 1637–1653 (1987).
15. R. Kurz, M. Schulz, F. Scheliga, Y. Men, A. Seidlitz, T. Thurn-Albrecht, K. Saalwächter, Interplay between crystallization and entanglements in the amorphous phase of the crystal-fixed polymer poly(ε-caprolactone). *Macromolecules* **51**, 5831–5841 (2018).
16. M. Schulz, A. Seidlitz, R. Kurz, R. Bärenwald, A. Petzold, K. Saalwächter, T. Thurn-Albrecht, The underestimated effect of intracrystalline chain dynamics on the morphology and stability of semicrystalline polymers. *Macromolecules* **51**, 8377–8385 (2018).
17. A. Keller, D. J. Priest, Experiments on the location of chain ends in monolayer single crystals of polyethylene. *J. Macromol. Sci. Part B Phys.* **2**, 479–495 (1968).
18. A. P. M. Kentgens, E. de Boer, W. S. Veeman, Ultraslow molecular motions in crystalline polyoxymethylene. A complete elucidation using two-dimensional solid state NMR. *J. Chem. Phys.* **87**, 6859–6866 (1987).
19. N. M. Robert, Polyoxymethylenes, US2768994A (1956).
20. D. Braun, H. Cherdron, M. Rehan, H. Ritter, B. Voit, *Polymer Synthesis: Theory and Practice: Fundamentals, Methods, Experiments* (Springer, 2004).
21. S. Hara, K. Yamamoto, S. Okamoto, S. Shimada, M. Sakaguchi, Molecular mobility of an amorphous chain in the crystallization process of poly(ε-caprolactone). *Macromolecules* **37**, 5323–5326 (2004).
22. J. Schaefer, E. O. Stejskal, R. A. McKay, W. T. Dixon, Molecular motion in polycarbonates by dipolar rotational spin-echo Carbon-13 NMR. *Macromolecules* **17**, 1479–1489 (1984).
23. K. Schmidt-Rohr, J. Clauss, H. W. Spiess, Correlation of structure, mobility, and morphological information in heterogeneous polymer materials by two-dimensional wideline-separation NMR spectroscopy. *Macromolecules* **25**, 3273–3277 (1992).
24. M. G. Menges, J. Penelle, C. Le Fevere de Ten Hove, A. M. Jonas, K. Schmidt-Rohr, Characterization of long-chain aliphatic polyesters: Crystalline and supramolecular structure of PE22,4 elucidated by X-ray scattering and nuclear magnetic resonance. *Macromolecules* **40**, 8714–8725 (2007).
25. S.-F. Liu, J.-D. Mao, K. Schmidt-Rohr, A robust technique for two-dimensional separation of undistorted chemical-shift anisotropy powder patterns in magic-angle-spinning NMR. *J. Magn. Reson.* **155**, 15–28 (2002).
26. J. D. Mao, K. Schmidt-Rohr, Separation of aromatic-carbon ^{13}C NMR signals from di-oxygenated alkyl bands by a chemical-shift-anisotropy filter. *Solid State Nucl. Magn. Reson.* **26**, 36–45 (2004).
27. K. Saalwächter, Proton multiple-quantum NMR for the study of chain dynamics and structural constraints in polymeric soft materials. *Prog. Nucl. Magn. Reson. Spectrosc.* **51**, 1–35 (2007).
28. K. Schmidt-Rohr, H. W. Spiess, *Multidimensional Solid-State NMR and Polymers* (Academic Press, 1994).
29. E. R. deAzevedo, W.-G. Hu, T. J. Bonagamba, K. Schmidt-Rohr, Centerband-only detection of exchange: Efficient analysis of dynamics in solids by NMR. *J. Am. Chem. Soc.* **121**, 8411–8412 (1999).
30. W. S. Veeman, E. M. Menger, W. Ritchey, E. de Boer, High-resolution carbon-13 nuclear magnetic resonance of solid poly(oxymethylene). *Macromolecules* **12**, 924–927 (1979).
31. U. Haeberlen, *High Resolution NMR in Solids Selective Averaging* (Elsevier, 1976).
32. K. K. Kumashiro, K. Schmidt-Rohr, O. J. Murphy, K. L. Ouellette, W. A. Cramer, L. K. Thompson, A novel tool for probing membrane protein structure: Solid-State NMR with proton spin diffusion and X-nucleus detection. *J. Am. Chem. Soc.* **120**, 5043–5051 (1998).
33. Y.-l. Hong, W. Chen, S. Yuan, J. Kang, T. Miyoshi, Chain trajectory of semicrystalline polymers as revealed by solid-state NMR spectroscopy. *ACS Macro Lett.* **5**, 355–358 (2016).
34. D. Reichert, T. J. Bonagamba, K. Schmidt-Rohr, Slow-down of ^{13}C spin diffusion in organic solids by fast MAS: A CODEX NMR study. *J. Magn. Reson.* **151**, 129–135 (2001).
35. D. M. Gezovich, P. H. Geil, Deformation of polyoxymethylene by rolling. *J. Mater. Sci.* **6**, 509–530 (1971).
36. F. Khoury, J. D. Barnes, The formation of curved polymer crystals: Polyoxymethylene. *J. Res. Natl. Stand. A Phys. Chem.* **78A**, 95–127 (1974).
37. R. C. Savage, N. Mullin, J. K. Hobbs, Molecular conformation at the crystal–amorphous interface in polyethylene. *Macromolecules* **48**, 6160–6165 (2015).
38. X. Zeng, G. Ungar, S. J. Spells, S. M. King, Real-time neutron scattering study of transient phases in polymer crystallization. *Macromolecules* **38**, 7201–7204 (2005).
39. P. Duan, K. Schmidt-Rohr, Composite-pulse and partially dipolar dephased multiCP for improved quantitative solid-state ^{13}C NMR. *J. Magn. Reson.* **285**, 68–78 (2017).
40. M. Goldman, L. Shen, Spin-spin relaxation in LaF_3. *Phys. Rev.* **144**, 321–331 (1966).
41. N. Egger, K. Schmidt-Rohr, B. Blümich, W. D. Domke, B. Stapp, Solid state NMR investigation of cationic polymerized epoxy resins. *J. Appl. Polym. Sci.* **44**, 289–295 (1992).
42. W. Luo, M. Hong, Determination of the oligomeric number and intermolecular distances of membrane protein assemblies by anisotropic ^{1}H-driven spin diffusion NMR spectroscopy. *J. Am. Chem. Soc.* **128**, 7242–7251 (2006).
43. E. Moreno, R. Cordobilla, T. Calvet, F. J. Lahoz, A. I. Balana, The C form of n-hexadecanoic acid. *Acta Crystallogr. C* **62**, o129–o131 (2006).

Acknowledgments: S.Y. thanks Bokai Xu and I. Krauss for providing the initiator for the polymerization and K. Saalwächter, T. Miyoshi, and B. Lotz for helpful discussions. **Funding:** The spectrometer used in this work was funded by the NSF MRI program, award no. 1726346.
Author contributions: Both authors planned the project, executed NMR measurements, analyzed data, and wrote the manuscript. S.Y. synthesized ^{13}C-Ac_2-POM and performed CODEX and spin diffusion simulations. **Competing interests:** The authors declare that they have no competing interests. **Data and materials availability:** All data needed to evaluate the conclusions in the paper are present in the paper and/or the Supplementary Materials. Additional data related to this paper may be requested from the authors.

Submitted 1 April 2020
Accepted 20 July 2020
Published 11 September 2020
10.1126/sciadv.abc0059

Citation: S. Yuan, K. Schmidt-Rohr, Immobilized ^{13}C-labeled polyether chain ends confined to the crystallite surface detected by advanced NMR. *Sci. Adv.* **6**, eabc0059 (2020).